Title

Selective activation of parvalbumin interneurons prevents stress-induced synapse loss and perceptual defects.

Journal

Molecular psychiatry, 23(7)

ISSN

1359-4184

Authors

Chen, C-C
Lu, J
Yang, R
et al.

Publication Date

2018-07-01

DOI

10.1038/mp.2017.159

Peer reviewed

HHS Public Access

Author manuscript

Mol Psychiatry. Author manuscript; available in PMC 2018 February 02.

Selective activation of parvalbumin interneurons prevents stress-induced synapse loss and perceptual defects

Chia-Chien Chen, PhD[1], **Ju Lu, PhD**[1], **Renzhi Yang, BS**[2], **Jun B. Ding, PhD**[2,3], and **Yi Zuo, PhD**[1,*]

[1]Department of Molecular, Cell and Developmental Biology, University of California, Santa Cruz, CA 95064, USA

[2]Department of Neurosurgery, Stanford University School of Medicine, Palo Alto, CA 94304, USA

[3]Department of Neurology and Neurological Sciences, Stanford University School of Medicine, Palo Alto, CA 94304, USA

Abstract

Stress, a prevalent experience in modern society, is a major risk factor for many psychiatric disorders. Although sensorimotor abnormalities are often present in these disorders, little is known about how stress affects the sensory cortex. Combining behavioral analyses with *in vivo* synaptic imaging, we show that stressful experiences lead to progressive, clustered loss of dendritic spines along the apical dendrites of layer (L) 5 pyramidal neurons (PNs) in the mouse barrel cortex, and such spine loss closely associates with deteriorated performance in a whisker-dependent texture discrimination task. Furthermore, the activity of parvalbumin-expressing inhibitory interneurons (PV+ INs) decreases in the stressed mouse due to reduced excitability of these neurons. Importantly, both behavioral defects and structural changes of L5 PNs are prevented by selective pharmacogenetic activation of PV+ INs in the barrel cortex during stress. Finally, stressed mice raised under environmental enrichment (EE) maintain normal activation of PV+ INs, normal texture discrimination, and L5 PN spine dynamics similar to unstressed EE mice. Our findings suggest that the PV+ inhibitory circuit is crucial for normal synaptic dynamics in the mouse barrel cortex and sensory function. Pharmacological, pharmacogenetic, and environmental approaches to prevent stress-induced maladaptive behaviors and synaptic malfunctions converge on the regulation of PV+ IN activity, pointing to a potential therapeutic target for stress-related disorders.

INTRODUCTION

Ample clinical data have established a strong link between psychological stress and mental illnesses[1, 2]. Stress adversely affects many brain functions, as evidenced by the wide spectrum of affective and cognitive abnormalities it induces (*e.g.*, anxiety, social avoidance, anhedonia, and memory impairment)[3, 4]. It represents a predominant risk factor for many

Correspondence: Dr. Yi Zuo, Department of Molecular, Cell and Developmental Biology, University of California, Santa Cruz, CA 95064, USA, yizuo@ucsc.edu, Phone: +1-831-459-3812, Fax: +1-831-459-3139.

Conflict of Interest: The authors declare no conflict of interest.

psychiatric disorders, including generalized anxiety disorder, major depressive disorder, bipolar disorder, and post-traumatic stress disorder[5, 6]. To date, the majority of research on stress focuses on its emotional and social aspects[7]; far less is known regarding its effect on basic cortical functions such as sensorimotor processing.

Previous research on stress-induced structural changes in the brain has revealed abnormalities in dendritic morphology and in dendritic spines (as a proxy of excitatory synapses[8, 9]) of excitatory neurons. For example, chronic restraint stress (RS) causes dendritic atrophy and spine loss in the hippocampus[10], which correlates with decreased hippocampal volume in patients of stress-related disorders[11]. Stressed animals exhibit similar dendritic and spine defects in the prefrontal cortex (PFC)[12, 13]. These data suggest that synaptic dysregulation underlies the pathophysiology of stress-induced functional deficits. Nevertheless, all these studies were performed on fixed tissues. Although they provide invaluable knowledge about the endpoint of chronic stress, they could not resolve how stress-induced synaptic defects develop. Specifically, information is lacking about how synaptic dynamics are altered in the presence of stressors in live animals.

Although inhibitory neurons represent only 20–30% of neurons in the mature cortex, they are essential components of brain circuits and participate in various neural computations[14, 15]. Many neurological and psychiatric disorders (*e.g.*, autism spectrum disorders and schizophrenia) implicate an imbalance between the actions of excitatory and inhibitory neurons[16–20]. In particular, PV+ INs are the predominant interneurons in the cortex[21]. They innervate the target PNs perisomatically, therefore exerting powerful inhibition[22, 23]. However, it is unclear whether stress alters cortical PV+ INs and their associated circuits, and how such effects contribute to stress-induced synaptic remodeling and behavioral defects.

The road to recovery from stress poses important questions for both basic and clinical neuroscience. EE is beneficial to normal brain function[24] and in many disease models, including amblyopia[25], Alzheimer's disease[26], epilepsy[27], and the Fragile X Syndrome[28]. Recent studies also suggest that EE accelerates post-stress reversal and promotes resilience to stress[29–31]. However, it remains unclear how EE affects synaptic plasticity and local cortical circuits, and whether such effects differ on normal and stressed brains. Exploring the mechanisms of experience-dependent rescue for stress is important, because it may guide the development and incorporation of non-pharmacological supportive therapies for stress-related diseases.

MATERIALS AND METHODS

Experimental animals

Adolescent mice, around 1 month of age, were used for most experiments unless otherwise noted. *Thy1*-YFP H[32] (JAX #003782) and PV-Cre[33] (JAX #008069) mouse lines were purchased from the Jackson Laboratory and maintained in the C57BL/6J background. Heterozygous PV-Cre mice and wild type mice were used in pharmacogenetic experiments. Mice were group-housed in the UCSC animal facility, with 12 h light-dark cycle and access

to food and water *ad libitum*. All procedures were performed in accordance with protocols approved by the Animal Care and Use Committee (IACUC) of UCSC.

Stress protocols

Both male and female mice were used in the experiments, starting at one month of age. RS was imposed by placing the mouse in a perforated 50 ml conical tube for 2 h daily, as previously described[34]. Littermates were randomly assigned to the stress or the control group. Unpredictable mild stress (UMS) was administered to each cohort of mice in a weekly-rotating schedule, as previously described[35].

Whisker-dependent texture discrimination task

The whisker-dependent texture discrimination task was modified from a previously described protocol[36]. The timeline of the experiment is shown in Supplementary Figure 2a. The mouse was individually habituated in a 38 cm × 28 cm × 23 cm opaque plexiglass box with bedding ("arena") for 10 min per day for 2 d. On the third (testing) day, the mouse was first given 3 min to explore the arena (*i.e.*, exploration phase), then temporarily (< 30 s) removed to allow the placement of two columns (3 cm × 3 cm × 9 cm) with identically textured surfaces. The mouse was then returned to the arena and given 5 min to familiarize itself with the texture of the two columns (*i.e.*, encoding phase). If the mouse showed insufficient interest in the columns (*i.e.*, < 16 total approaches) or biased towards one column (*i.e.*, > 60% approaching time spent on one column), it was excluded from further testing. Otherwise, the mouse was removed for another 5 min to allow the two columns to be replaced by two new columns, one with the habituated texture and the other with a novel texture. The mouse was given 3 min to explore and interact with the new columns (*i.e.*, testing phase). In each experiment, either the 220 grits or the 1500 grits sandpaper (Ace Hardware, Inc) was randomly selected as the habituated or the novel texture. Mouse behavior was recorded with an iPad Air 2; the video files were exported to Noldus Ethovision 10.11 for analysis. The software tracked the X–Y coordinates of the mouse's nose-point throughout the video at 10 frames per second and generated a composite positional map. The total amount of time the mouse spent approaching each column was measured, and the discrimination index was calculated as previously described[37]. For stressed mice, habituation started on the antepenultimate day of stress, and testing started 2 h after the final stress session. In a separate set of experiments, instead of textured columns, objects differing in non-texture features (*e.g.*, shape and color) were used to assess short-term memory[38].

Environmental enrichment

EE mice were reared in groups of 4 to 8 in large cages containing various toys (*e.g.*, tunnels, bells, ropes, ladders, and running wheels) as previously described[39]. Control mice were housed in standard mouse cages, with up to 5 mice per cage but never alone.

In vivo transcranial imaging and quantification

Transcranial two-photon imaging and spine dynamics analyses were performed as described previously[40, 41]. Dendritic segments (> 10 μm long) with high image quality in both imaging

sessions were identified and dendritic spines were tracked manually along the dendrites from 3D stacks in ImageJ. To analyze dendritic tip retraction and interspine distances, dendritic segments and spines were manually traced in Neurolucida 11.0 (MBF Biosciences); dendritic length differences and interspine distances were calculated from tracing results in Neuroexplorer 11.0 (MBF Biosciences). Spine clustering was analyzed with custom-written codes in MATLAB R2013a (MathWorks). Instances of two or more adjacent spines eliminated together were counted as clustered spine elimination. The actual clustering probability was calculated as the total number of clustered eliminations divided by the total number of spines on all dendritic segments. To generate the frequency distribution of clustering probabilities, we randomly selected on each dendritic segment exactly the same number of spines as were actually eliminated from that segment, and computed the clustered elimination probability from the simulated dataset. This scheme took into consideration the fact that under different experimental conditions, the clustering probabilities under the null hypothesis (random elimination) vary due to the differences in the rate of spine elimination. The simulation was repeated 50,000 times. Finally we compared the actual clustering probability to the corresponding frequency distribution.

Immunohistochemistry and image quantification

Stressed mice were perfused approximately 2.5 h after the cessation of the final stress session. Perfusion and immunohistochemistry were performed as previously described[42]. The following primary antibodies were used: rabbit-anti-cFos (ab5, Calbiochem, 1:10000), rabbit-anti-cFos (226-003, Synaptic Systems, 1:10000), mouse-anti-cFos (sc-166940, Santa Cruz Biotech, 1:200), mouse-anti-parvalbumin (MAB1572, Millipore, 1:1000), rat-anti-somatostatin (MAB354, Millipore, 1:500), rabbit-anti-neurogranin (AB5620, Millipore, 1:1000), rabbit-anti-GFP (A11122, ThermoFisher Scientific, 1:1000), rabbit-anti-mCherry (EMU106, Kerafast, 1:2000). The following secondary antibodies were used: biotinylated goat-anti-rabbit or goat-anti-mouse (Vector Laboratories, 1:200), AlexaFluor 488/594-conjugated goat-anti-mouse, goat-anti-rat, or goat-anti-rabbit (ThermoFisher, 1:500). For all c-Fos immunolabeling, biotinylated secondary antibodies were used, followed by Alexa 488- or 594-conjugated streptavidin (ThermoFisher, 1:500) to enhance the signal, as previously described[43]. All sections were counterstained with 4′-6-Diamidino-2-phenylindole (DAPI; 1:36,000), air-dried, submerged in 100% ethanol for 1 min, then coverslipped with Vectashield (Hardset, Vector Laboratories).

Confocal images were taken with a Leica TCS-SP5 microscope under 20× NA 0.75 air or 40× NA 1.25 oil-immersion objectives. Brain-wide images were obtained on a Keyence BZ-9000 microscope under a 10× NA 0.45 air objective. For cell counting and colocalization analyses, image stacks were obtained on a Zeiss Imager M2 microscope equipped with a Hamamatsu Orca-ER digital camera under a 20× NA 0.8 air objective. StereoInvestigator/Neurolucida 11.0 was used to quantify cell density and colocalization as previously described[44].

Slice electrophysiology

Brain slices (300 μm) were obtained from 1-month-old mice using standard techniques[45]. L5 PNs were visualized under infrared illumination using an Olympus BX-51 microscope

equipped with DIC optics, a water-immersion objective (60× NA 1.1), and a CMOS camera (Hamamatsu Photonics). YFP+ neurons were identified under epifluorescence illumination (Lambda XL, Sutter Instrument). Whole-cell voltage-clamp recording was performed with borosilicate glass microelectrodes (3–5 MΩ) filled with a Cs^+-based low Cl^- internal solution (126 mM $CsCH_3SO_3$, 8 mM NaCl, 10 mM HEPES, 2.9 mM QX-314, 8 mM Na_2-Phosphocreatine, 0.3 mM Na_2GTP, 4 mM MgATP, 0.1 mM $CaCl_2$, 1 mM EGTA; pH 7.2–7.3; osmolarity 285–290 mOsm). The access resistance was < 25MΩ (no compensation), and the data were discarded if the access resistance changed more than 20% during recording. For recording miniature EPSCs (mEPSCs) and miniature IPSCs (mIPSCs), TTX (1 μM) was included to prevent action potential firing. For evoked EPSC and IPSCs, TTX was omitted and stimulation (100–200 μs) was delivered using steel concentric electrodes (FHC, Bowdoin) placed 100–200 μm to the somata of L5 PNs. To measure both IPSCs and EPSCs from the same neuron, the membrane potential was first held at +4 mV (the reversal potential of ionotropic glutamate receptors, liquid junction potential not corrected) to measure IPSCs and then at −70 mV (the reversal potential of Cl^-) to measure EPSCs. To examine the overall strength of inhibition mediated by PV+ INs, we injected AAV5-EF1a-DIO-ChR2-mCherry into the barrel cortex of PV-Cre mice on postnatal day (P) 0, and prepared coronal brain slices on P37. We performed whole-cell voltage clamp recording on PNs and delivered a brief (0.2 ms) blue light stimulation using a 450 nm laser (OptoEngine, USA). The laser was focused at the back aperture of the objective to achieve full field illumination. In order to measure the peak amplitude of optogenetically evoked IPSCs (oIPSCs) in PNs, we gradually increased the blue light intensity until the oIPSC amplitude plateaued (< 10% increase with 2–3 folds increase in laser intensity). To assess the excitability of PV+ INs, we identified them by mCherry expression and performed whole-cell current clamp recordings with a K^+-based internal solution (135 mM KCH_3SO_3, 8.1 mM KCl, 10 mM HEPES, 8 mM Na_2-Phosphocreatine, 0.3 mM Na_2GTP, 4 mM MgATP, 0.1 mM $CaCl_2$, 1 mM EGTA; pH 7.2–7.3; osmolarity: 285–290 mOsm). To measure the firing of PV+ INs, incremental current steps (2 s duration, 30 pA step size) were injected through the recording pipette. Recordings were obtained with a Multiclamp 700B amplifier (Molecular Devices) using the WinWCP software (University of Strathclyde, UK). Signals were filtered at 2 kHz, digitized at 10 kHz (NI PCIe-6259, National Instruments), and analyzed offline using Clampfit 10.0 (Molecular Devices) and Mini Analysis Program (Synaptosoft).

Viral injection and pharmacogenetic manipulation

AAV8-hSyn-DIO-hM3Dq-mCherry (DREADD virus), AAV8-CaMKIIa-hM3Dq-mCherry (CaMKII DREADD virus), AAV8-CAG-FLEX-GFP (control GFP virus) and AAV5-EF1a-DIO-mCherry (control mCherry virus) were purchased from the University of North Carolina Vector Core. AAV5-EF1a-DIO-hChR2(H134R)-mCherry was purchased from the University of Pennsylvania Vector Core. For virus validation, P14 PV-Cre mice were anesthetized with intraperitoneal injection of ketamine-xylazine (100 mg ketamine/10 mg xylazine per kg body weight); 300 nl DREADD virus or control GFP virus were pressure-injected (50 nl/min) using a custom-built injection system based on a Narishige single-axis oil hydraulic micromanipulator (Narishige, Tokyo, Japan) into the barrel cortices (AP: −0.5 mm, ML: 2.5 mm). To infect a large population of neurons in the barrel cortex, neonatal

(P0–1) PV-Cre mice were anesthetized by ice-induced hypothermia as previously described[46]. 200 nl of DREADD virus or control mCherry virus were injected (50 nl/min) into the barrel cortices bilaterally (AP: −0.2 mm, ML: 2.0 mm). 4 weeks of incubation were allowed before behavioral, imaging, and immunohistochemical experiments. For pharmacogenetic manipulations, CNO was dissolved in sterile saline and injected intraperitoneally at 0.3 mg/kg body weight[47], 15 min prior to RS. For vehicle control, saline was injected at the same time point instead.

Statistical analyses

All behavioral, spine dynamics, immunohistochemical, and electrophysiological data were analyzed with the analyst blinded to the experimental conditions. Details of behavioral, spine and dendritic tip dynamics, and immunohistochemical data are itemized by experimental conditions, together with the number and sex of mice used for each condition, and given in Supplementary Tables 1–4. All statistical analyses were performed using Statistica 12.0 and SPSS 23.0. Data from each mouse were treated as a single data point in a group unless otherwise noted. We performed the Shapiro-Wilk test for sample normality, and examined the homogeneity of variance. If assumptions were met for parametric tests, Student's *t*-test were used for two groups, and Analysis of Variance (ANOVA) followed by *post hoc* Tukey HSD test was used for three or more groups. Otherwise, the Mann-Whitney U-test was used for non-matched two-sample comparison, and the Kruskal-Wallis test followed by Conover test with Holm Family-Wide Error Rate (FWER) *p*-value adjustment was used for three or more groups. Analysis of Covariance (ANCOVA) was used to test the linear relationship between the evoked EPSCs and IPSCs.

Code availability

Custom-written MATLAB codes are available upon request.

RESULTS

Stress impairs the whisker-dependent texture discrimination ability of mice

Mice depend on their whiskers, highly specialized peripheral tactile detectors, to explore the environment. The sensory input from whiskers is transmitted to the barrel cortex for further processing[48, 49]. To determine how stress affects whisker-dependent sensory functions, we subjected mice to RS for 2 h daily from 2 to 14 days, and then assessed their performance in a whisker-dependent texture discrimination task (Figure 1a,b). Control mice spent significantly more time approaching the column with the novel texture than that with the habituated texture (Figure 1c,d). This required intact whiskers and the barrel cortex, as mice with bilateral whisker trimming or barrel cortex lesion exhibited no preference for the novel texture (Supplementary Figure 1). We also found that RS progressively deteriorated the texture discrimination performance: 2-day RS led to detectable impairment, and 7- or 14-day RS completely abolished the ability to distinguish the two textures. Similar behavioral defects were also observed in mice experiencing 14 days of UMS (Figure 1e), and no sex difference was found in this behavior ($p>0.2$ for both control and 7-day RS). Furthermore, such defects were not due to reduced whisker length, increased anxiety, altered exploratory

behavior, or short-term memory loss (Supplementary Information, Supplementary Figures 2, 3).

Stress induces progressive spine loss in the mouse barrel cortex

As the integrity of the barrel cortex is necessary for the texture discrimination task (Supplementary Figure 1b,c), we asked how RS affects neuronal circuits therein. To visualize neurons *in vivo*, we used the *thy1*-YFP H line mice, in which a small subset of cortical L5 PNs express cytoplasmic yellow fluorescent protein (YFP)[32]. We imaged the same set of apical dendrites of L5 PNs in the barrel cortices of RS mice over different time intervals using transcranial two-photon microscopy[40, 41]. Control mice exhibited 7.8% spine formation and 13.2% spine elimination over the 7-day period. Spine elimination in RS mice was almost twice as much as in control mice ($p<0.001$). In contrast, spine formation was unperturbed by RS ($p>0.8$, Figure 1f,g). The onset of elevated spine elimination was rapid (observable with 2-day RS), and continued RS further aggravated spine loss, *i.e.*, more spines were eliminated during the 8th and 9th day of RS than during the initial two days (Figure 1h, $p<0.001$). Furthermore, elevated spine elimination persisted even after the cessation of RS. After 7 days of stress, mice continued to exhibit significantly higher spine elimination over the 2-day recovery period than controls (Figure 1h, $p<0.001$). Spine loss was also observed after prolonged stress (14-day RS or UMS, $p<0.001$ for both compared to control, Figure 1i). Finally, stress-induced increase in spine elimination is not limited to the barrel cortex, as similar changes were observed in the visual cortex of stressed mice (Supplementary Figure 4).

As the spatial configuration of spines impacts postsynaptic signal integration[50, 51], we analyzed the distribution of spines along linearized dendritic segments. We measured the relative locations of 1336 spines (199 eliminated) along 64 dendritic segments from 5 control mice, and 1363 spines (411 eliminated) along 59 dendritic segments from 7 mice after 7-day RS. Based on these measurements, we quantified the instances of clustered spine elimination, *i.e.*, two or more adjacent spines eliminated together (Figure 1j,l), and computed the clustering probability. To test whether the observed clustering probability represents a tendency towards clustered elimination rather than arising by chance, we compared it to the prediction of a uniform elimination model generated by the Monte Carlo method. We found that under control conditions, the observed clustering probability (3.29%) did not exceed chance level (*i.e.*, less than the 95th percentile of the cumulative distribution; Figure 1k). In contrast, in RS mice spines were significantly more likely to be eliminated in clusters than predicted by the null model (*i.e.*, above the 95th percentile of the cumulative distribution; Figure 1m).

Previous fixed tissue studies have also shown that stress causes PN dendritic atrophy in the hippocampus and the PFC[10, 52]. To determine the temporal order of dendritic tip retraction and spine loss, we examined apical dendrites of L5 PNs *in vivo*. We found a progressive retraction of dendritic tips from 2 to 14 days in both control and RS mice. While the amount of tip retraction was comparable between control and RS mice over 2-day period ($p>0.9$), 7-day and 14-day RS significantly increased tip retraction ($p<0.05$ for 7-day, $p<0.001$ for 14-day, Supplementary Figure 5). Comparing the timeline of tip retraction with that of spine

loss suggests that stress-induced increase in dendritic spine loss precedes dendritic atrophy in L5 PNs.

Stress decreases the activity of PV+ INs and increases the activity of excitatory neurons in the mouse barrel cortex

Inhibitory interneurons regulate activity-dependent neuronal circuit development, sensory processing, and synaptic functions[53–55]. Recent evidence suggests that stress induces hypo-activity of inhibitory interneurons and hyper-activity of excitatory neurons in the amygdala and the hippocampus[56, 57]; whether this effect generalizes to cortical areas remains unknown. Thus we examined the expression of the immediate early gene c-Fos in the barrel cortex of control and RS mice. As c-Fos is upregulated in neurons after they fire action potentials, its expression is considered a good proxy of recent neuronal activation[58, 59]. We found that the density of c-Fos+ cells in the barrel cortex was significantly higher in mice that underwent 7-day RS than in controls ($p<0.001$, Figure 2a,b). To better understand the activation of distinct neuronal populations, we co-labeled c-Fos with either neurogranin (NG, an excitatory neuron marker)[60] or PV. We found that the overall density and laminar distribution of NG+ neurons and PV+ INs remained unchanged (Figure 2c–f, Supplementary Figure 5a,b). However, 7-day RS doubled the percentage of NG+ neurons that were c-Fos+ ($p<0.001$), and halved the percentage of PV+ INs that were c-Fos+ ($p<0.001$; Figure 2g–j). This was consistent across all the cortical layers examined (L2–L5, Supplementary Figure 6). In addition, a single RS session did not alter the density of c-Fos+ neurons, nor did it affect the activity of NG+ neurons or PV+ INs (Supplementary Figure 7a–c). Furthermore, the intensity of PV correlated with that of c-Fos and decreased significantly in the 7-day RS mice (Supplementary Figure 7d). These data suggest that stress shifts the network excitation-inhibition balance in the barrel cortex towards hyper-excitation.

Stress alters the balance between excitatory and inhibitory inputs onto L5 PNs in the barrel cortex

To reveal how stress impacts excitatory and inhibitory synaptic transmission, we recorded α-amino-3-hydroxy-5-methyl-4-isoxazolepropionic acid receptor (AMPAR) mediated spontaneous miniature excitatory postsynaptic currents (mEPSCs) and gamma-aminobutyric acid A receptor ($GABA_AR$) mediated spontaneous miniature inhibitory postsynaptic currents (mIPSCs) from YFP+ L5 PNs in control and RS *thy1*-YFP H mice using whole-cell voltage clamp. We found that RS did not significantly change either mEPSC frequency or amplitude (Figure 3a,c,e), nor was there significant difference in mIPSC frequency and amplitude between control and RS mice (Figure 3b,d,f). These data suggest that RS does not change presynaptic vesicular release probability or the number of active glutamatergic and GABAergic synapses formed onto L5 PNs. Unperturbed mIPSCs, together with reduced number of PV+ INs that were c-Fos+, suggests that the recruitment of perisomatic inhibition may be reduced in RS mice. Therefore, we asked whether this stress-induced population-level excitation-inhibition imbalance manifests itself at the level of synaptic inputs to a single neuron. To detect relative excitatory and inhibitory synaptic strength, we delivered electric stimulations in L5 and recorded evoked EPSCs and IPSCs (eEPSCs and eIPSCs) from L5 PNs (Figure 3g). Because the amplitudes of eEPSCs and eIPSCs are highly variable depending on the placement of the stimulation electrode, we recorded both eEPSCs and

eIPSCs under the same stimulation conditions by switching holding potentials. In both control and 7d RS mice, the amplitudes of eIPSCs and eEPSCs increased with the stimulation intensity. The ratio between eIPSC and eEPSC amplitude stayed relatively constant, shown as comparable slopes of linear regression fit of eIPSC and eEPSC amplitudes (Figure 3h). However, given an eEPSC amplitude, the size of corresponding eIPSCs was significantly reduced in 7d RS mice compared to controls, leading to a down-shift of the linear I-E curve and significantly lowering the y-intercept of the linear regressions ($p<0.0001$, Figure 3h). This is consistent with the decreased activity of PV+ INs (Figure 2j). Together, these data suggest that stress shifts the stimulation evoked synaptic balance onto L5 PNs towards hyper-excitation in the barrel cortex.

Next we asked whether the decreased eIPSCs were due to decreased synaptic connections from PV+ INs onto PNs. We injected AAV5-EF1a-DIO-hChR2(H134R)-mCherry into the barrel cortex of PV-Cre mice at P0, and recorded the optogenetically evoked IPSCs (oIPSCs) in P37 coronal slices from either control or 7d RS mice. We found that the peak amplitude of oIPSCs was comparable between stressed and control mice (Figure 3i,j), indicating that the overall synaptic strength from PV+ INs onto PNs is not altered by stress, consistent with our mIPSC data. This suggests that the decreased relative eIPSCs in the stressed mice may arise from decreased excitability of PV+ INs. To test this hypothesis, we directly recorded from PV+ INs in L5 of the barrel cortex. We found that the frequency of action potentials fired by PV+ INs in response to current injection is lower in stressed mice than in controls (Figure 3k,l). Such data suggest decreased PV+ IN excitability in the stressed brain, and are consistent with the reduced c-Fos labeling in PV+ INs.

Pharmacological enhancement of inhibitory synaptic transmission or attenuation of excitatory transmission prevents stress-induced synaptic and behavioral defects

As the stressed cortex exhibits hyper-excitation, we asked whether enhancing inhibitory or attenuating excitatory synaptic transmission can prevent stress-induced anatomical and functional alterations. To decrease excitatory synaptic transmission, we systemically administered MK801, a non-competitive N-methyl-D-aspartate receptor (NMDAR) antagonist, before each RS session for 7 days. MK801 has been shown to attenuate spine elimination rate *in vivo*[61], and can reverse stress-induced spine loss to control levels[62]. To enhance inhibitory synaptic transmission, we intraperitoneally injected diazepam, a $GABA_AR$ agonist, into RS mice before each stress session. Earlier work has shown that enhancing $GABA_AR$ suffices to block stress-induced dendritic atrophy and spine loss[63], and to prevent stress-induced c-Fos over-activation[64]. We found that spine elimination rate was significantly lower in RS mice treated with either MK801 or diazepam than in untreated RS mice (both $p<0.001$), but comparable to that in control mice (Supplementary Figure 8a). Interestingly, drug-treated RS mice performed normally in the texture discrimination task ($p>0.7$ for both vs. non-stressed control, Supplementary Figure 8b). In addition, RS mice treated with either drug showed significantly lower global neuronal activation and higher PV + IN activation than untreated RS mice (both $p<0.05$, Supplementary Figure 8c–e), suggesting that dosing mice with MK801 or diazepam prevents RS-induced disruption of neuronal excitation-inhibition balance.

Pharmacogenetic restoration of PV+ IN activity in stressed mice prevents stress-induced synaptic and behavioral defects

As systemic drug administration lacks regional or cell-type specificity, we next tested whether selectively enhancing PV+ IN activity in the barrel cortex counteracts stress-induced hyper-excitation. We took advantage of the Designer Receptors Exclusively Activated by Designer Drugs (DREADDs)[65]. We infected cortical neurons in PV-Cre mice with adeno-associated virus encoding the mutant human muscarinic receptor Gq (AAV8-DIO-Syn-hm3q-mCherry, "DREADD virus"), and activated DREADD virus-infected neurons with Clozapine-N-Oxide (CNO), a synthetic hm3q agonist. To test the specificity and efficiency of the DREADD system, we injected DREADD virus and AAV8-CAG-Flex-GFP virus ("control GFP virus") into the barrel cortices on opposite hemispheres of the same PV-Cre mouse on postnatal day 14 (P14). Approximately 95% of the neurons labeled by either DREADD or control GFP virus were PV+ (Figure 4a,b), which confirms the selective targeting of PV+ INs. After a single dose of CNO, immunohistochemical staining for c-Fos was positive in more than 95% of DREADD virus-infected neurons, a percentage significantly higher than that of control GFP virus-infected neurons (Figure 4c,d, $p<0.001$). These data demonstrate that the DREADD system can selectively activate mouse cortical PV + INs *in vivo*.

To manipulate the activity of PV+ INs in the stressed mice, we injected DREADD virus bilaterally into the barrel cortex of PV-Cre mice at P0 or P1. After incubation for 1 month, we injected CNO or saline into these mice before each daily RS session (Figure 4e,f). We found significantly fewer c-Fos+ cells in CNO-treated mice ("DREADD+CNO") than in saline-treated mice ("DREADD+saline") after 7-day RS (Supplementary Figure 9a $p<0.05$). Specifically, the percentage of virus-infected PV+ INs that were c-Fos+ was significantly higher in DREAD+CNO RS mice than in DREADD+saline RS mice ($p<0.05$, Figure 4g). We also examined the percentage of NG+ cells that were activated following DREADD activation of PV+ INs in stressed mice. We found that 14% NG+ cells were c-Fos+, which was significantly lower than that in stressed mice without rescue ($p<0.05$, Supplementary Figure 9b). In addition, DREADD+CNO RS mice exhibited normal spine dynamics ($p>0.2$ for both spine formation and elimination compared to control unstressed mice), dendritic tip retraction ($p>0.4$ comparing to control) and performance in texture discrimination ($p>0.2$ compared to control), whereas AAV5-EF1a-DIO-mCherry virus (control mCherry virus) infection with CNO treatment or DREADD+saline had no effect on either spine dynamics or task performance of RS mice (both $p>0.3$ compared to 7d RS, Figure 4h,I, Supplementary Figure 9c). Furthermore, DREADD-mediated activation of PV+ INs outside the barrel cortex did not rescue the texture discrimination defect in RS mice (Supplementary Figure 10). These data suggest that stress-induced PV+ IN hypofunction in the barrel cortex is a culprit of synaptic dysregulation and sensory abnormalities in the stressed mice. Although PV+ INs represent only a small fraction of all cortical neurons, the effect of changes in their activity is amplified via the consequent prevention of over-activation of excitatory neurons, the majority of active cells in the cortex.

EE alleviates stress-induced synaptic and behavioral defects through activation of PV+ INs

Exposure to EE confers profound benefits to the brain, including accelerated post-stress reversal and resilience to stress[29–31]. We sought to determine whether EE can also prevent stress-induced spine loss and sensory impairment. Immunohistochemical staining of c-Fos showed increased activation of NG+ neurons in mice raised under EE (EE mice), compared to those raised in standard cages (control mice; $p<0.05$, Figure 5a,c). In EE mice, daily stress did not further change the percentage of activated NG+ neurons ($p>0.9$, Figure 5c), nor did it reduce PV+ IN activity ($p>0.1$ vs. control, $p>0.6$ vs. EE, Figure 5b, Supplementary Figure 7d). In contrast, RS increased the activation of somatostatin-expressing (SOM+) INs, which was not prevented by EE (Figure 5d). Furthermore, EE mice had a higher rate of spine formation and elimination over 7 days compared to control mice ($p<0.05$ for both elimination and formation, Figure 5e,f), and the effect of daily RS on spine elimination was occluded ($p>0.7$, Figure 5f). Spine elimination in both EE and EE+RS mice was significantly lower compared with non-EE RS mice ($p<0.01$ for both). RS did not increase the dendritic tip retraction in EE mice (Supplementary Figure 12a), as opposed to control mice. More importantly, while EE alone did not alter the mouse's performance in the texture discrimination task, EE+RS mice were as competent as both control and unstressed EE mice ($p>0.8$; Figure 5g, Supplementary Figure 11b). Together, these data reveal that EE prevents stress-induced hyper-excitation in the cortex and synaptic/behavioral defects.

DISCUSSION

Human studies have reported that acute physical and psychological stress adversely affects auditory[66] and visual processing[67]. In addition, fear, which is presumably stressful, reduces tactile sensitivity[68]. Stress is also a predominant risk factor for many anxiety and depressive disorders[5, 6]. In addition to the emotional problems, sensorimotor abnormalities are often present in depression[69]. Clinical data indicate that patients with major depression have decreased volume and surface area of somatosensory cortex and abnormal sensory processing[70, 71]. Our study examines the cellular underpinning of sensory alterations caused by psychological stress in a mouse model. Combining behavioral analysis, *in vivo* imaging, and local circuit dissection, we provide a possible mechanism through which stress affects cortical circuits and sensory function.

Previous studies on fixed brain tissues have reported that stress leads to decreased spine density and shorter dendritic arborization in brain regions such as the hippocampus and the PFC[10, 12, 52]. However it is unclear whether the reduced spine density is due to decreased spinogenesis or increased spine loss. Our *in vivo* two-photon imaging experiments filled this knowledge gap by clarifying that stress increases spine elimination without affecting spine formation. Interestingly, spine elimination tends to cluster along dendrites, suggesting a local regulatory mechanism. Analogous clustered structural dynamics has been reported previously on spine formation. One study on hippocampal organotypic cultures found that most newly formed spines preferentially grow in close proximity to activated synapses, leading to a clustering of functional synapses[72]. Subsequent *in vivo* imaging experiments revealed clustered spine formation in response to motor skill learning[39], as well as clustered formation between excitatory and inhibitory synapses[73]. The mechanisms underlying such

clustered reorganization of dendritic spines may depend on the postsynaptic milieu or presynaptic elements. On the postsynaptic side, clustering could be due to the diffusion of intracellular signaling molecules such as guanosine triphosphatases (GTPase) Ras[74] and RhoA[75]. Synaptic activity may also trigger molecular signaling that acts on neighboring spines, as suggested by heterosynaptic structural and functional depression[76]. Alternatively, spines may compete for limited cellular resources, such as the postsynaptic scaffolding protein PSD-95[77] and cadherin/catenin cell adhesion complexes[78]. On the presynaptic side, the geometric arrangement of local axons may dictate the observed spine clustering, as dendrites can only form synapses with axonal branches within a short distance. In addition, axons synapsing onto adjacent spines may originate from the same ensemble of neurons and share similar activities[79–81], which may drive clustered postsynaptic structural dynamics through activity-dependent plasticity rules. Previous fixed tissue studies also show that stress causes atrophy of apical dendrites in the PFC[13, 82], which is consistent with our finding. Furthermore, our study reveals that the accelerated dendritic spine loss precedes dendritic tip retraction in the stressed brain, suggesting that synaptic degradation happens before neuronal atrophy. It is also worth noting that we focused on one-month old mice. Previous studies suggest an age-dependence in stress reactivity and recovery[82], such that adolescents may be more susceptible to stress than adults but also recover faster[83]. Thus it would be rewarding for future studies to explore the age-dependent responses to stress in brain regions underlying sensorimotor functions.

The complex effect of stress on excitatory synapses involves neuroendocrine factors such as glucocorticoids (GCC) and the corticotropin-releasing hormone (CRH). Administration of GCC enhances dendritic spine turnover in the developing barrel cortex, whereas reducing endogenous GCC activity substantially reduces spine turnover[84]. Various proteins in the actin regulatory pathways mediate the effect of GCC on synaptic structure and plasticity[85, 86]. CRH destabilizes dendritic spines via a glutamate receptor-mediated process[62]. Blocking CRH receptor 1 ameliorates early-life stress-induced dendritic and synaptic abnormalities in the neonatal hippocampus[87]. Mice with CRH receptor deficiency in the forebrain exhibits attenuated cognitive deficits and dendritic remodeling in response to chronic stress[88].

How the brain processes external stimuli depends on its internal state[89, 90]. In addition to the well-recognized role played by neuromodulators in controlling brain states[89, 91], it is increasingly clear that the delicate interactions between local excitation and inhibition are important for gain control in sensory processes and neural plasticity[53, 55]. Our data suggest that stress significantly reduces the recruitment of PV+ INs, but does not alter presynaptic vesicular release probability or the number of active GABAergic synapses formed on L5 PNs. This hypo-inhibition is concomitant with hyper-activity of excitatory neurons, which may in turn lead to the loss of dendritic spines thereon via a homeostatic mechanism[92]. Corroborating this idea is the finding that direct activation of excitatory neurons induced spine elimination (Supplementary Figure 12). Furthermore, such hypo-inhibition may increase cortical noise and disrupt sensory processing, as the state of inhibitory circuits is crucial for fine texture detection[93, 94]. Indeed, hypofunction of GABAergic transmission is present in stress-induced abnormal behaviors and psychiatric disorders in human patients[95]. Our study demonstrates that stress-induced structural and functional defects can be

prevented by pharmacological or behavioral intervention that regulates PV+ IN activity, suggesting a preventative strategy for stress-induced psychiatric disorders.

It is noteworthy that NG immunohistochemistry likely labels only a subset of excitatory neurons. We examined the percentage of c-Fos+ cells that are NG+, PV+, or SOM+, and found that under control condition, NG+ cells account for 56% of c-Fos+ cells, while PV+ cells account for 5.6%. Following 7d stress, the percentages change to 48% (NG+) and 1.1% (PV+). This leaves 40–50% of c-Fos+ cells unaccounted for. This discrepancy cannot be simply attributed to other types of INs, as they collectively constitute less than 20% of all cortical neurons (Supplementary Figure 13). Furthermore, c-Fos+ cells are predominantly neurons, as suggested by co-immunostaining with the pan-neuronal marker NeuN (data not shown). Therefore, we believe that NG immunohistochemistry only labels a subset of excitatory neurons, and the unlabeled excitatory neurons also contribute significantly to the increase in c-Fos+ cells.

In conclusion, we found that stress reduces PV+ IN activation, accelerates spine loss, alters global neuronal excitation-inhibition in the primary somatosensory cortex, and hence profoundly affects sensory processing. Pharmacogenetic and behavioral manipulations that enhance PV+ IN activity can prevent stress-induced spine loss and over-excitation. Nevertheless, it is important to note that the stress-induced cellular changes may involve complex feedback interactions among neuronal circuit elements either sequentially or in parallel. Given this complexity, it is intriguing that modulating PV+ INs alone suffices to reverse the deficits. The exact nature of stress-induced cellular alterations, as well as a comprehensive picture of all contributing types of cells, remains to be deciphered in future studies.

Supplementary Material

Refer to Web version on PubMed Central for supplementary material.

Acknowledgments

We gratefully thank Drs. Caitlin Moyer, Joshua Brumberg and James Ackman for critical comments on this manuscript, and Fernando Serrano, Mason Lee and Sajita Shah-Morales for technical support. This work was supported by grants from the National Institute of Mental Health (R01MH104227 and R01MH109475), National Institute of Neurological Disorders and Stroke (R01NS078791) to Y.Z. and (R01NS091144) to J.B.D. and QB3-Calico to Y.Z.

References

1. de Kloet ER, Joels M, Holsboer F. Stress and the brain: from adaptation to disease. Nat Rev Neurosci. 2005; 6(6):463–475. [PubMed: 15891777]
2. Schmitt A, Malchow B, Hasan A, Falkai P. The impact of environmental factors in severe psychiatric disorders. Front Neurosci. 2014; 8:19. [PubMed: 24574956]
3. Krishnan V, Han MH, Graham DL, Berton O, Renthal W, Russo SJ, et al. Molecular adaptations underlying susceptibility and resistance to social defeat in brain reward regions. Cell. 2007; 131(2): 391–404. [PubMed: 17956738]
4. Chen Y, Rex CS, Rice CJ, Dube CM, Gall CM, Lynch G, et al. Correlated memory defects and hippocampal dendritic spine loss after acute stress involve corticotropin-releasing hormone signaling. Proc Natl Acad Sci U S A. 2010; 107(29):13123–13128. [PubMed: 20615973]

5. Kendler KS, Karkowski LM, Prescott CA. Causal relationship between stressful life events and the onset of major depression. Am J Psychiatry. 1999; 156(6):837–841. [PubMed: 10360120]
6. Staufenbiel SM, Penninx BW, Spijker AT, Elzinga BM, van Rossum EF. Hair cortisol, stress exposure, and mental health in humans: a systematic review. Psychoneuroendocrinology. 2013; 38(8):1220–1235. [PubMed: 23253896]
7. Beery AK, Kaufer D. Stress, social behavior, and resilience: insights from rodents. Neurobiol Stress. 2015; 1:116–127. [PubMed: 25562050]
8. Harris KM, Kater SB. Dendritic spines: cellular specializations imparting both stability and flexibility to synaptic function. Annu Rev Neurosci. 1994; 17:341–371. [PubMed: 8210179]
9. Nimchinsky EA, Sabatini BL, Svoboda K. Structure and function of dendritic spines. Annu Rev Physiol. 2002; 64:313–353. [PubMed: 11826272]
10. Magarinos AM, Li CJ, Gal Toth J, Bath KG, Jing D, Lee FS, et al. Effect of brain-derived neurotrophic factor haploinsufficiency on stress-induced remodeling of hippocampal neurons. Hippocampus. 2011; 21(3):253–264. [PubMed: 20095008]
11. Savitz J, Drevets WC. Bipolar and major depressive disorder: neuroimaging the developmental-degenerative divide. Neurosci Biobehav Rev. 2009; 33(5):699–771. [PubMed: 19428491]
12. Radley JJ, Rocher AB, Rodriguez A, Ehlenberger DB, Dammann M, McEwen BS, et al. Repeated stress alters dendritic spine morphology in the rat medial prefrontal cortex. J Comp Neurol. 2008; 507(1):1141–1150. [PubMed: 18157834]
13. Radley JJ, Sisti HM, Hao J, Rocher AB, McCall T, Hof PR, et al. Chronic behavioral stress induces apical dendritic reorganization in pyramidal neurons of the medial prefrontal cortex. Neuroscience. 2004; 125(1):1–6. [PubMed: 15051139]
14. Markram H, Toledo-Rodriguez M, Wang Y, Gupta A, Silberberg G, Wu C. Interneurons of the neocortical inhibitory system. Nat Rev Neurosci. 2004; 5(10):793–807. [PubMed: 15378039]
15. Druga R. Neocortical inhibitory system. Folia Biol (Praha). 2009; 55(6):201–217. [PubMed: 20163769]
16. Yizhar O, Fenno LE, Prigge M, Schneider F, Davidson TJ, O'Shea DJ, et al. Neocortical excitation/inhibition balance in information processing and social dysfunction. Nature. 2011; 477(7363):171–178. [PubMed: 21796121]
17. Gogolla N, Leblanc JJ, Quast KB, Sudhof TC, Fagiolini M, Hensch TK. Common circuit defect of excitatory-inhibitory balance in mouse models of autism. J Neurodev Disord. 2009; 1(2):172–181. [PubMed: 20664807]
18. Lisman J. Excitation, inhibition, local oscillations, or large-scale loops: what causes the symptoms of schizophrenia? Curr Opin Neurobiol. 2012; 22(3):537–544. [PubMed: 22079494]
19. Markram K, Markram H. The intense world theory - a unifying theory of the neurobiology of autism. Front Hum Neurosci. 2010; 4:224. [PubMed: 21191475]
20. Lewis DA. Inhibitory neurons in human cortical circuits: substrate for cognitive dysfunction in schizophrenia. Curr Opin Neurobiol. 2014; 26:22–26. [PubMed: 24650500]
21. Rudy B, Fishell G, Lee S, Hjerling-Leffler J. Three groups of interneurons account for nearly 100% of neocortical GABAergic neurons. Dev Neurobiol. 2011; 71(1):45–61. [PubMed: 21154909]
22. Kubota Y, Kawaguchi Y. Dependence of GABAergic synaptic areas on the interneuron type and target size. J Neurosci. 2000; 20(1):375–386. [PubMed: 10627614]
23. Somogyi P, Kisvarday ZF, Martin KA, Whitteridge D. Synaptic connections of morphologically identified and physiologically characterized large basket cells in the striate cortex of cat. Neuroscience. 1983; 10(2):261–294. [PubMed: 6633861]
24. van Praag H, Kempermann G, Gage FH. Neural consequences of environmental enrichment. Nat Rev Neurosci. 2000; 1(3):191–198. [PubMed: 11257907]
25. Tognini P, Manno I, Bonaccorsi J, Cenni MC, Sale A, Maffei L. Environmental enrichment promotes plasticity and visual acuity recovery in adult monocular amblyopic rats. PLoS One. 2012; 7(4):e34815. [PubMed: 22509358]
26. Jankowsky JL, Melnikova T, Fadale DJ, Xu GM, Slunt HH, Gonzales V, et al. Environmental enrichment mitigates cognitive deficits in a mouse model of Alzheimer's disease. J Neurosci. 2005; 25(21):5217–5224. [PubMed: 15917461]

27. Faverjon S, Silveira DC, Fu DD, Cha BH, Akman C, Hu Y, et al. Beneficial effects of enriched environment following status epilepticus in immature rats. Neurology. 2002; 59(9):1356–1364. [PubMed: 12427884]
28. Restivo L, Ferrari F, Passino E, Sgobio C, Bock J, Oostra BA, et al. Enriched environment promotes behavioral and morphological recovery in a mouse model for the fragile X syndrome. Proc Natl Acad Sci U S A. 2005; 102(32):11557–11562. [PubMed: 16076950]
29. Francis DD, Diorio J, Plotsky PM, Meaney MJ. Environmental enrichment reverses the effects of maternal separation on stress reactivity. J Neurosci. 2002; 22(18):7840–7843. [PubMed: 12223535]
30. Lehmann ML, Herkenham M. Environmental enrichment confers stress resiliency to social defeat through an infralimbic cortex-dependent neuroanatomical pathway. J Neurosci. 2011; 31(16): 6159–6173. [PubMed: 21508240]
31. Cooper MA, Clinard CT, Morrison KE. Neurobiological mechanisms supporting experience-dependent resistance to social stress. Neuroscience. 2015; 291:1–14. [PubMed: 25677096]
32. Feng G, Mellor RH, Bernstein M, Keller-Peck C, Nguyen QT, Wallace M, et al. Imaging neuronal subsets in transgenic mice expressing multiple spectral variants of GFP. Neuron. 2000; 28(1):41–51. [PubMed: 11086982]
33. Hippenmeyer S, Vrieseling E, Sigrist M, Portmann T, Laengle C, Ladle DR, et al. A developmental switch in the response of DRG neurons to ETS transcription factor signaling. PLoS Biol. 2005; 3(5):e159. [PubMed: 15836427]
34. Seo JS, Park JY, Choi J, Kim TK, Shin JH, Lee JK, et al. NADPH oxidase mediates depressive behavior induced by chronic stress in mice. J Neurosci. 2012; 32(28):9690–9699. [PubMed: 22787054]
35. Schweizer MC, Henniger MS, Sillaber I. Chronic mild stress (CMS) in mice: of anhedonia, 'anomalous anxiolysis' and activity. PLoS One. 2009; 4(1):e4326. [PubMed: 19177164]
36. Wu HP, Ioffe JC, Iverson MM, Boon JM, Dyck RH. Novel, whisker-dependent texture discrimination task for mice. Behav Brain Res. 2013; 237:238–242. [PubMed: 23026377]
37. Okuda S, Roozendaal B, McGaugh JL. Glucocorticoid effects on object recognition memory require training-associated emotional arousal. Proc Natl Acad Sci U S A. 2004; 101(3):853–858. [PubMed: 14711996]
38. Antunes M, Biala G. The novel object recognition memory: neurobiology, test procedure, and its modifications. Cogn Process. 2012; 13(2):93–110. [PubMed: 22160349]
39. Fu M, Yu X, Lu J, Zuo Y. Repetitive motor learning induces coordinated formation of clustered dendritic spines in vivo. Nature. 2012; 483(7387):92–95. [PubMed: 22343892]
40. Xu T, Yu X, Perlik AJ, Tobin WF, Zweig JA, Tennant K, et al. Rapid formation and selective stabilization of synapses for enduring motor memories. Nature. 2009; 462(7275):915–919. [PubMed: 19946267]
41. Zuo Y, Lin A, Chang P, Gan WB. Development of long-term dendritic spine stability in diverse regions of cerebral cortex. Neuron. 2005; 46(2):181–189. [PubMed: 15848798]
42. Hodges JL, Yu X, Gilmore A, Bennett H, Tjia M, Perna JF, et al. Astrocytic Contributions to Synaptic and Learning Abnormalities in a Mouse Model of Fragile X Syndrome. Biol Psychiatry. 2016
43. Chen CC, Chu P, Brumberg JC. Experience-dependent regulation of tissue-type plasminogen activator in the mouse barrel cortex. Neurosci Lett. 2015; 599:152–157. [PubMed: 26021877]
44. Barrera K, Chu P, Abramowitz J, Steger R, Ramos RL, Brumberg JC. Organization of myelin in the mouse somatosensory barrel cortex and the effects of sensory deprivation. Dev Neurobiol. 2013; 73(4):297–314. [PubMed: 23047707]
45. Ding J, Peterson JD, Surmeier DJ. Corticostriatal and thalamostriatal synapses have distinctive properties. J Neurosci. 2008; 28(25):6483–6492. [PubMed: 18562619]
46. De Marco Garcia NV, Priya R, Tuncdemir SN, Fishell G, Karayannis T. Sensory inputs control the integration of neurogliaform interneurons into cortical circuits. Nat Neurosci. 2015; 18(3):393–401. [PubMed: 25664912]

47. Krashes MJ, Koda S, Ye C, Rogan SC, Adams AC, Cusher DS, et al. Rapid, reversible activation of AgRP neurons drives feeding behavior in mice. J Clin Invest. 2011; 121(4):1424–1428. [PubMed: 21364278]
48. Fox K. Anatomical pathways and molecular mechanisms for plasticity in the barrel cortex. Neuroscience. 2002; 111(4):799–814. [PubMed: 12031405]
49. Erzurumlu RS, Gaspar P. Development and critical period plasticity of the barrel cortex. Eur J Neurosci. 2012; 35(10):1540–1553. [PubMed: 22607000]
50. Govindarajan A, Kelleher RJ, Tonegawa S. A clustered plasticity model of long-term memory engrams. Nat Rev Neurosci. 2006; 7(7):575–583. [PubMed: 16791146]
51. Larkum ME, Nevian T. Synaptic clustering by dendritic signalling mechanisms. Curr Opin Neurobiol. 2008; 18(3):321–331. [PubMed: 18804167]
52. Garrett JE, Wellman CL. Chronic stress effects on dendritic morphology in medial prefrontal cortex: sex differences and estrogen dependence. Neuroscience. 2009; 162(1):195–207. [PubMed: 19401219]
53. Lee SH, Kwan AC, Zhang S, Phoumthipphavong V, Flannery JG, Masmanidis SC, et al. Activation of specific interneurons improves V1 feature selectivity and visual perception. Nature. 2012; 488(7411):379–383. [PubMed: 22878719]
54. Fagiolini M, Fritschy JM, Low K, Mohler H, Rudolph U, Hensch TK. Specific GABAA circuits for visual cortical plasticity. Science. 2004; 303(5664):1681–1683. [PubMed: 15017002]
55. Atallah BV, Bruns W, Carandini M, Scanziani M. Parvalbumin-expressing interneurons linearly transform cortical responses to visual stimuli. Neuron. 2012; 73(1):159–170. [PubMed: 22243754]
56. MacKenzie G, Maguire J. Chronic stress shifts the GABA reversal potential in the hippocampus and increases seizure susceptibility. Epilepsy Res. 2015; 109:13–27. [PubMed: 25524838]
57. Liu ZP, Song C, Wang M, He Y, Xu XB, Pan HQ, et al. Chronic stress impairs GABAergic control of amygdala through suppressing the tonic GABAA receptor currents. Mol Brain. 2014; 7:32. [PubMed: 24758222]
58. Guzowski JF, Timlin JA, Roysam B, McNaughton BL, Worley PF, Barnes CA. Mapping behaviorally relevant neural circuits with immediate-early gene expression. Curr Opin Neurobiol. 2005; 15(5):599–606. [PubMed: 16150584]
59. Fields RD, Eshete F, Stevens B, Itoh K. Action potential-dependent regulation of gene expression: temporal specificity in ca2+, cAMP-responsive element binding proteins, and mitogen-activated protein kinase signaling. J Neurosci. 1997; 17(19):7252–7266. [PubMed: 9295372]
60. Singec I, Knoth R, Ditter M, Volk B, Frotscher M. Neurogranin is expressed by principal cells but not interneurons in the rodent and monkey neocortex and hippocampus. J Comp Neurol. 2004; 479(1):30–42. [PubMed: 15389613]
61. Zuo Y, Yang G, Kwon E, Gan WB. Long-term sensory deprivation prevents dendritic spine loss in primary somatosensory cortex. Nature. 2005; 436(7048):261–265. [PubMed: 16015331]
62. Andres AL, Regev L, Phi L, Seese RR, Chen Y, Gall CM, et al. NMDA receptor activation and calpain contribute to disruption of dendritic spines by the stress neuropeptide CRH. J Neurosci. 2013; 33(43):16945–16960. [PubMed: 24155300]
63. Magarinos AM, Deslandes A, McEwen BS. Effects of antidepressants and benzodiazepine treatments on the dendritic structure of CA3 pyramidal neurons after chronic stress. Eur J Pharmacol. 1999; 371(2–3):113–122. [PubMed: 10357248]
64. de Medeiros MA, Carlos Reis L, Eugenio Mello L. Stress-induced c-Fos expression is differentially modulated by dexamethasone, diazepam and imipramine. Neuropsychopharmacology. 2005; 30(7):1246–1256. [PubMed: 15714225]
65. Roth BL. DREADDs for Neuroscientists. Neuron. 2016; 89(4):683–694. [PubMed: 26889809]
66. Jafari Z, Kolb BE, Mohajerani MH. Effect of acute stress on auditory processing: a systematic review of human studies. Rev Neurosci. 2017; 28(1):1–13. [PubMed: 27718496]
67. Weckesser LJ, Alexander NC, Kirschbaum C, Mennigen E, Miller R. Hydrocortisone Counteracts Adverse Stress Effects on Dual-Task Performance by Improving Visual Sensory Processes. Journal of Cognitive Neuroscience. 2016; 28(11):1784–1803. [PubMed: 27378327]
68. Kelley NJ, Schmeichel BJ. The effects of negative emotions on sensory perception: fear but not anger decreases tactile sensitivity. Front Psychol. 2014; 5:942. [PubMed: 25202299]

69. Canbeyli R. Sensorimotor modulation of mood and depression: An integrative review. Behav Brain Res. 2010; 207(2):249–264. [PubMed: 19913058]
70. Schmaal L, Hibar DP, Samann PG, Hall GB, Baune BT, Jahanshad N, et al. Cortical abnormalities in adults and adolescents with major depression based on brain scans from 20 cohorts worldwide in the ENIGMA Major Depressive Disorder Working Group. Mol Psychiatry. 2016
71. Serafini G, Engel-Yeger B, Vazquez GH, Pompili M, Amore M. Sensory Processing Disorders are Associated with Duration of Current Episode and Severity of Side Effects. Psychiatry Investig. 2017; 14(1):51–57.
72. De Roo M, Klauser P, Muller D. LTP promotes a selective long-term stabilization and clustering of dendritic spines. PLoS Biol. 2008; 6(9):e219. [PubMed: 18788894]
73. Chen JL, Villa KL, Cha JW, So PT, Kubota Y, Nedivi E. Clustered dynamics of inhibitory synapses and dendritic spines in the adult neocortex. Neuron. 2012; 74(2):361–373. [PubMed: 22542188]
74. Harvey CD, Yasuda R, Zhong H, Svoboda K. The spread of Ras activity triggered by activation of a single dendritic spine. Science. 2008; 321(5885):136–140. [PubMed: 18556515]
75. Murakoshi H, Wang H, Yasuda R. Local, persistent activation of Rho GTPases during plasticity of single dendritic spines. Nature. 2011; 472(7341):100–104. [PubMed: 21423166]
76. Oh WC, Parajuli LK, Zito K. Heterosynaptic structural plasticity on local dendritic segments of hippocampal CA1 neurons. Cell Rep. 2015; 10(2):162–169. [PubMed: 25558061]
77. Gray NW, Weimer RM, Bureau I, Svoboda K. Rapid redistribution of synaptic PSD-95 in the neocortex in vivo. PLoS Biol. 2006; 4(11):e370. [PubMed: 17090216]
78. Bian WJ, Miao WY, He SJ, Qiu Z, Yu X. Coordinated Spine Pruning and Maturation Mediated by Inter-Spine Competition for Cadherin/Catenin Complexes. Cell. 2015; 162(4):808–822. [PubMed: 26255771]
79. Kleindienst T, Winnubst J, Roth-Alpermann C, Bonhoeffer T, Lohmann C. Activity-dependent clustering of functional synaptic inputs on developing hippocampal dendrites. Neuron. 2011; 72(6):1012–1024. [PubMed: 22196336]
80. Takahashi N, Kitamura K, Matsuo N, Mayford M, Kano M, Matsuki N, et al. Locally synchronized synaptic inputs. Science. 2012; 335(6066):353–356. [PubMed: 22267814]
81. Wilms CD, Hausser M. Reading out a spatiotemporal population code by imaging neighbouring parallel fibre axons in vivo. Nat Commun. 2015; 6:6464. [PubMed: 25751648]
82. Bloss EB, Janssen WG, McEwen BS, Morrison JH. Interactive effects of stress and aging on structural plasticity in the prefrontal cortex. J Neurosci. 2010; 30(19):6726–6731. [PubMed: 20463234]
83. Eiland L, Romeo RD. Stress and the developing adolescent brain. Neuroscience. 2013; 249:162–171. [PubMed: 23123920]
84. Liston C, Gan WB. Glucocorticoids are critical regulators of dendritic spine development and plasticity in vivo. Proc Natl Acad Sci U S A. 2011; 108(38):16074–16079. [PubMed: 21911374]
85. Jafari M, Seese RR, Babayan AH, Gall CM, Lauterborn JC. Glucocorticoid receptors are localized to dendritic spines and influence local actin signaling. Mol Neurobiol. 2012; 46(2):304–315. [PubMed: 22717988]
86. Tanokashira D, Morita T, Hayashi K, Mayanagi T, Fukumoto K, Kubota Y, et al. Glucocorticoid suppresses dendritic spine development mediated by down-regulation of caldesmon expression. J Neurosci. 2012; 32(42):14583–14591. [PubMed: 23077044]
87. Liao XM, Yang XD, Jia J, Li JT, Xie XM, Su YA, et al. Blockade of corticotropin-releasing hormone receptor 1 attenuates early-life stress-induced synaptic abnormalities in the neonatal hippocampus. Hippocampus. 2014; 24(5):528–540. [PubMed: 24493406]
88. Wang XD, Su YA, Wagner KV, Avrabos C, Scharf SH, Hartmann J, et al. Nectin-3 links CRHR1 signaling to stress-induced memory deficits and spine loss. Nat Neurosci. 2013; 16(6):706–713. [PubMed: 23644483]
89. Lee SH, Dan Y. Neuromodulation of brain states. Neuron. 2012; 76(1):209–222. [PubMed: 23040816]
90. Poulet JF, Petersen CC. Internal brain state regulates membrane potential synchrony in barrel cortex of behaving mice. Nature. 2008; 454(7206):881–885. [PubMed: 18633351]

91. Marder E. Neuromodulation of neuronal circuits: back to the future. Neuron. 2012; 76(1):1–11. [PubMed: 23040802]

92. Fauth M, Tetzlaff C. Opposing Effects of Neuronal Activity on Structural Plasticity. Front Neuroanat. 2016:10. [PubMed: 26903819]

93. Sachidhanandam S, Sermet BS, Petersen CC. Parvalbumin-Expressing GABAergic Neurons in Mouse Barrel Cortex Contribute to Gating a Goal-Directed Sensorimotor Transformation. Cell Rep. 2016

94. Siegle JH, Pritchett DL, Moore CI. Gamma-range synchronization of fast-spiking interneurons can enhance detection of tactile stimuli. Nat Neurosci. 2014; 17(10):1371–1379. [PubMed: 25151266]

95. Maddock RJ, Buonocore MH. MR spectroscopic studies of the brain in psychiatric disorders. Curr Top Behav Neurosci. 2012; 11:199–251. [PubMed: 22294088]

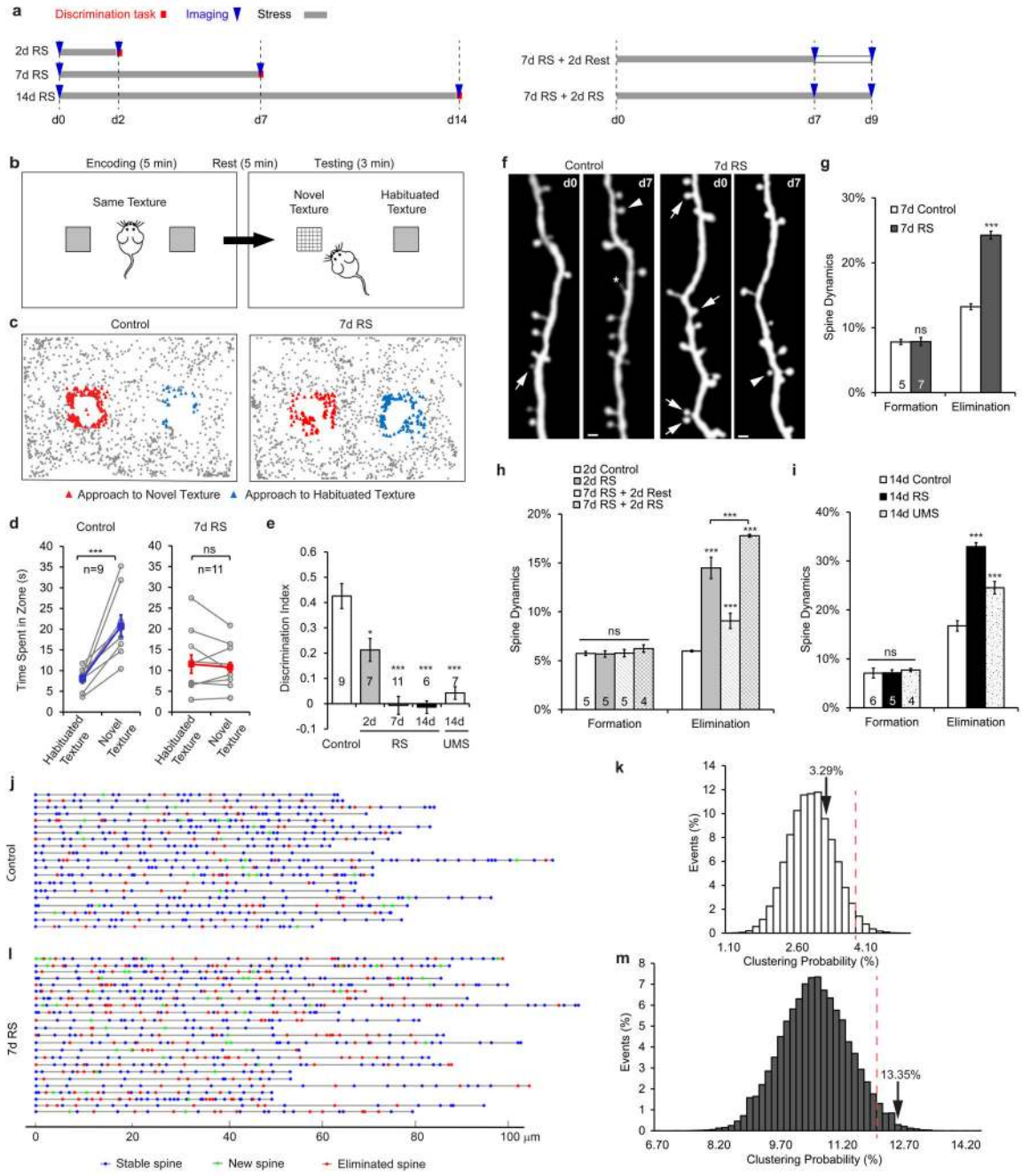

Figure 1. Stress induces progressive sensory impairment and spine loss in the mouse barrel cortex

a, Experimental design. RS: restraint stress. **b,** Setup of the whisker-dependent texture discrimination task. **c,** Representative positional maps of the mouse during the testing phase of the task. **d,** Control mice spent significantly longer time investigating the column with the novel texture than the column with the habituated texture; mice subjected to 7-day RS spent equal time investigating both columns. **e,** Stressed mice progressively lost the texture discrimination capability, shown as a decrease in the discrimination index. UMS: unpredictable mild stress. **f,** Repeated imaging of the same dendritic segments revealed spine

formation (arrowheads) and elimination (arrows) in control and RS mice. Asterisk indicates a dynamic filopodium. Scale bar: 2 μm. **g–i,** Spine elimination was increased in RS mice compared to controls, while spine formation was unperturbed. **j,i,** Dynamic dendro-spinogram revealed the location of spines that formed or disappeared over 7 days in control (**j**) and RS (**i**) mice. **k,m,** In RS mice, eliminated spines were significantly more likely to be clustered than predicted by a uniform, independent elimination model (**m**), whereas clustered elimination in control mice did not differ significantly from the model prediction (**k**). Arrows: observed probability of clustered eliminations. Red dotted lines mark the 95^{th}-percentile of the distribution of clustering probabilities derived from simulation. Hereinafter unless otherwise indicated, data are shown as mean ± standard error of the mean (s.e.m.), *p*-values represent a comparison to control mice without stress, and asterisks represent the following *p*-values: **p*<0.05, ***p*<0.01, ****p*<0.001.

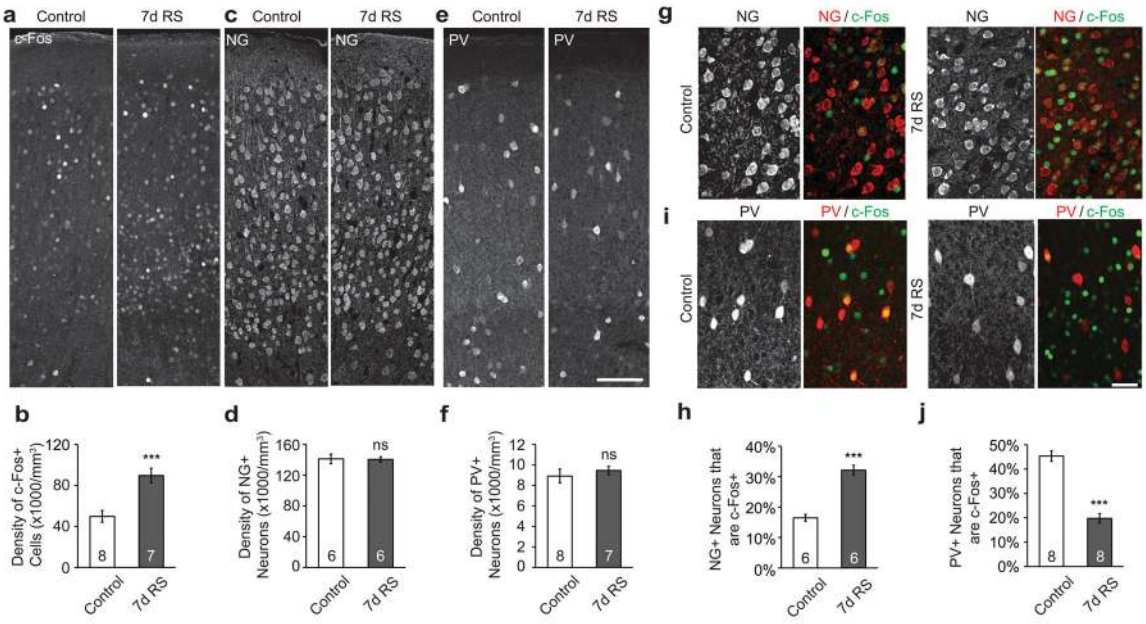

Figure 2. Stress decreases PV+ IN activity but increases excitatory neuron activity in the mouse barrel cortex

a, Examples of c-Fos immunofluorescence in coronal brain slices of control and 7-day RS mice. **b,** RS increased neuronal activation in the barrel cortex, as more cells were c-Fos immunoreactive. **c–f,** RS did not alter the density of NG+ neurons (**c,d**) or PV+ INs (**e,f**). **g,** An example of NG+ neurons with positive c-Fos immunofluorescence. **h,** RS increased the percentage of NG+ neurons that were colabeled with c-Fos. **i,** An example of PV+ INs colabeled with c-Fos. **j,** RS decreased the percentage of PV+ INs that were colabeled with c-Fos. Scale bars: 100 μm (**a,c,e**), 50 μm (**g,i**).

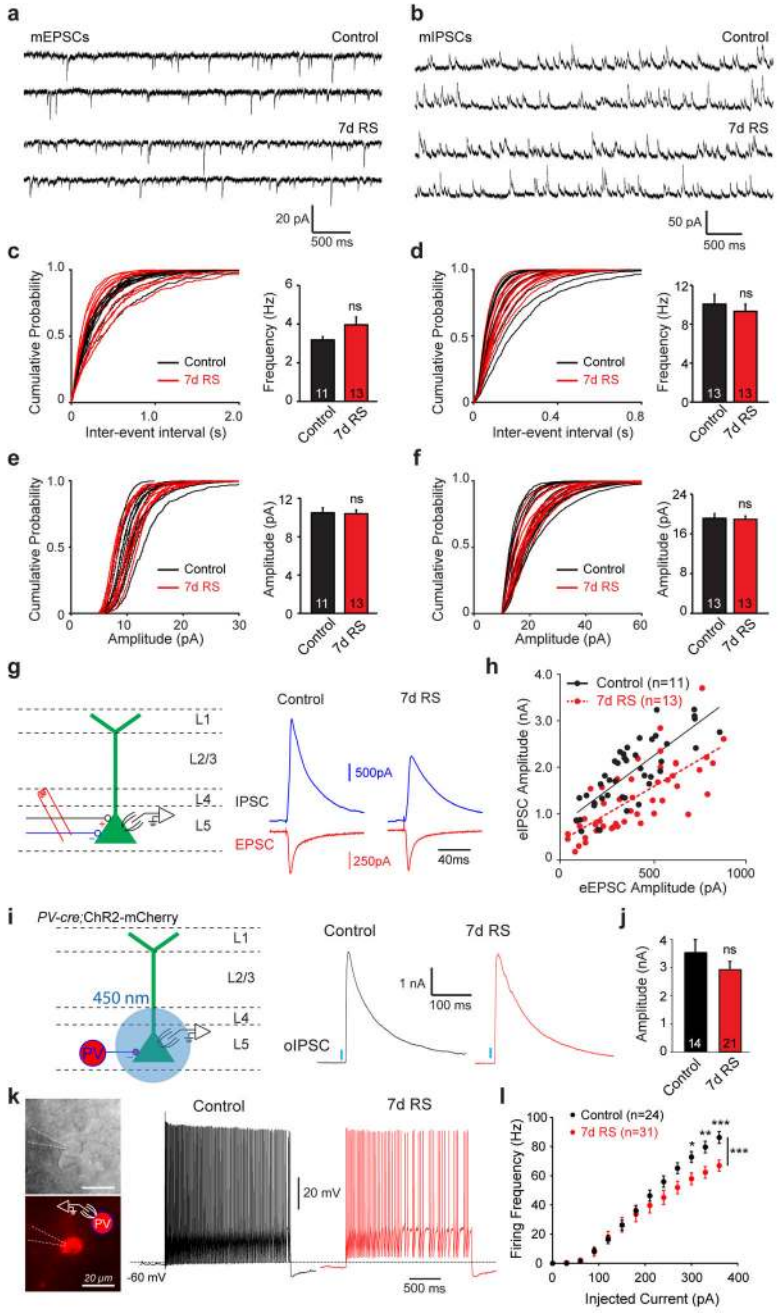

Figure 3. Stress alters the balance between excitatory and inhibitory inputs onto L5 PNs

a,b, Sample mEPSC (**a**) and mIPSC (**b**) recordings from control and 7-d RS mice. **c,d,** *Left*, cumulative probability distribution of inter-event intervals of mEPSCs (**c**) and mIPSCs (**d**) recorded from control and 7d RS mice. *Right*, frequency of mEPSC (**c**) and mIPSC (**d**) in control and RS mice. **e,f,** *Left*, cumulative probability distribution of amplitudes of mIPSCs (**e**) and mIPSCs (**f**) recorded from control and 7d RS mice. *Right*, amplitude of mEPSC (**e**) and mIPSC (**f**). **g,h,** Stress decreased eIPSC amplitude relative to eEPSC amplitude of L5 PNs in the barrel cortex. **g,** *Left*, schematic of electrophysiological experiments. The stimulation electrode was placed in L5 near the cell body. *Right*, sample traces of eEPSCs

and eIPSCs recorded from the same L5 PN in control and 7d RS mice. **h,** eIPSC amplitudes plotted against eEPSC amplitudes recorded from the same L5 PNs evoked by the same stimulation intensity. Lines: linear regression fits. The slope is not significantly different, but the y-intercept is (p<0.0001). **i,** *Left,* schematic of experiments. AAV-DIO-ChR2-mCherry was injected into the barrel cortex of PV-Cre mice, and oIPSCs evoked optogenetically with a 450 nm laser was recorded by whole-cell voltage-clamp. *Right,* sample traces of the maximal oIPSCs recorded in PNs from control and stressed mice. **j,** Amplitudes of the maximal oIPSCs evoked in control and stressed mice. **k–l,** Stress decreased intrinsic excitability of PV+ INs in the barrel cortex. **k,** *Left*, IR-DIC and epifluorescence images of an mCherry-expressing PV+ IN under whole-cell recording. *Right*, sample traces in response to a 300-pA current step from the control and stressed mice. **l,** Action potential firing frequency plotted against current injection for PV+ INs from control and 7d RS mice. *n* indicates the number of cells recorded.

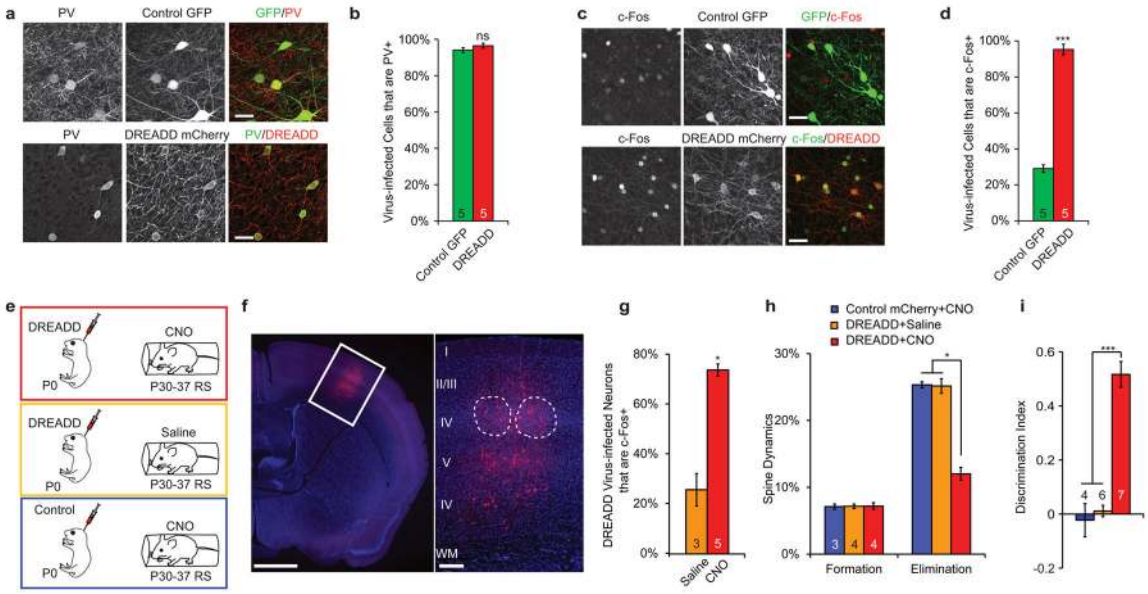

Figure 4. Restoration of PV+ IN activity in RS mice alleviates stress-induced spine loss and texture discrimination defects

a,b, PV immunohistochemistry showed that the majority of neurons infected by DREADD virus or control GFP virus were PV+ INs. **c,d**, A single dose of CNO selectively activated DREADD virus-infected neurons as shown by c-Fos immunohistochemistry. **e,** Experimental design of virus injection and drug treatment during stress. **f,** An example of DREADD virus infection targeting the barrel cortex. Dotted contours mark individual barrels in L4. **g,** DREADD virus-infected neurons in RS mice receiving CNO injection were significantly more active than those in RS mice receiving saline injection. **h,i,** DREADD +CNO prevented elevated spine elimination (**h**) and texture discrimination defects (**i**) caused by RS. Scale bars: 25 μm (**a,c**), 1 mm and 250 μm (**f**).

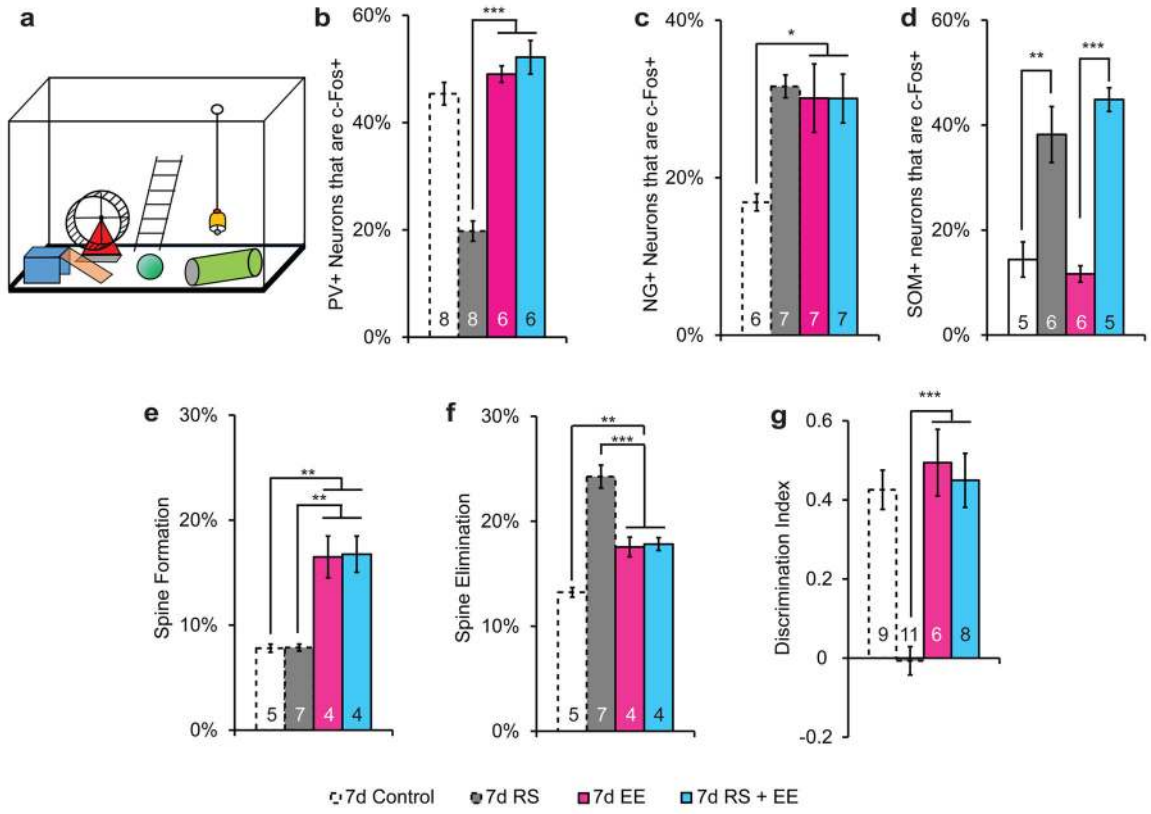

Figure 5. Mice raised under EE are resistant to stress-induced spine loss and texture discrimination defects

a, Schematic of EE. **b,** EE prevented RS-induced decrease in PV+ IN activity. **c**, Both stressed and unstressed EE mice had elevated activation of NG+ neurons compared to unstressed, non-EE control mice. **d**, Stress increased SOM+ neuron activation in both control and EE mice; EE had no effect on SOM+ neuron activation. **e,f,** EE increased both spine formation (**e**) and elimination (**f**) compared to unstressed, non-EE control mice. Stress did not further alter spine dynamics in EE mice. **g,** Both stressed and unstressed EE mice exhibited normal texture discrimination.